

CrystEngComm

Accepted Manuscript



This is an *Accepted Manuscript*, which has been through the Royal Society of Chemistry peer review process and has been accepted for publication.

Accepted Manuscripts are published online shortly after acceptance, before technical editing, formatting and proof reading. Using this free service, authors can make their results available to the community, in citable form, before we publish the edited article. We will replace this *Accepted Manuscript* with the edited and formatted *Advance Article* as soon as it is available.

You can find more information about *Accepted Manuscripts* in the [Information for Authors](#).

Please note that technical editing may introduce minor changes to the text and/or graphics, which may alter content. The journal's standard [Terms & Conditions](#) and the [Ethical guidelines](#) still apply. In no event shall the Royal Society of Chemistry be held responsible for any errors or omissions in this *Accepted Manuscript* or any consequences arising from the use of any information it contains.

Manifestation of intrinsic defects in band structure of quaternary chalcogenide $\text{Ag}_2\text{In}_2\text{SiSe}_6$ and $\text{Ag}_2\text{In}_2\text{GeSe}_6$ crystals

Cite this: DOI: 10.1039/x0xx00000x

Received 00th January 2012,
Accepted 00th January 2012

DOI: 10.1039/x0xx00000x

www.rsc.org/

M. Makowska-Janusik,^a I. V. Kityk,^b G. Myronchuk,^c O. Zamuraeva^c and O. V. Parasyuk^c,

The complex studies of the band structure for the novel $\text{Ag}_2\text{In}_2\text{SiSe}_6$ and $\text{Ag}_2\text{In}_2\text{GeSe}_6$ crystals were performed. For the first time a possibility to analyze experimentally and theoretically the manifestation of the intrinsic vacancies possessing cationic and anionic character located in quaternary crystals was shown. The contribution of the localized states into the band structure, optical absorption edge, effective masses, carrier mobility etc. was explored including both measurements of their polarized absorption fundamental edge as well as the electronic properties calculations within a framework of the DFT methodology. Therefore, the probability of different type of defect's appearance was analyzed and the dispersion of the energy band possessing substantial anisotropy of the carriers transport was discussed. Particularly were considered silver vacancies changing the energy gap of both crystal by adding the acceptor level above the valence band. The proposed approach may be generalized for many chalcogenide complexes.

Introduction

Quaternary crystals $\text{Ag}_2\text{In}_2\text{GeSe}_6$ and $\text{Ag}_2\text{In}_2\text{SiSe}_6$ have potential application in infrared optoelectronics, quantum electronics, light emitting diodes and solar systems as the promising narrow-gap semiconductor materials^{1,2}. The mentioned crystals were synthesized for the first time more than ten years ago by Krykhovets et al.³ and by Oleksyuk et al.⁴ but they never been widely investigated experimentally nor theoretically. These materials belong to the systems $\text{A}^{\text{I}}\text{-B}^{\text{III}}\text{-C}^{\text{IV}}\text{-X}^{\text{VI}}$, where generally $\text{A}^{\text{I}}=\text{Cu, Ag}$; $\text{B}^{\text{III}}=\text{Ga, In}$; $\text{C}^{\text{IV}}=\text{Ge, Si}$ and $\text{X}^{\text{VI}}=\text{S, Se}$. Currently, five chalcogenide complexes of the $\text{A}_2\text{In}_2\text{C}^{\text{IV}}\text{X}^{\text{VI}}_2$ type possessing the monoclinic structure are known⁵. An acentricity of the crystal structures of mentioned chalcogenides is one of the reasons to forecast their possible application also as non-linear optical material⁶⁻⁸. Though, one of a restraining factor for their further application as an optoelectronic and quantum electronic material is an existence of the intrinsic defects substantially disturbing the order

parameters of material as well as changing the band energy dispersions closely related to the carrier density. The different kind of localized vacancies form a very flat quasi-discrete energy levels effectively interacting with the delocalized states of the energy band creating their superposition leading to the substantial changes in the corresponding inter-band transition dipole moments^{9,10}. The chalcogenide complexes possess a rare coexistence of the cation and anion vacancies with different polarizabilities and therefore they can be selected as an exemplary model materials representing the group of $\text{A}_2\text{In}_2\text{C}^{\text{IV}}\text{X}^{\text{VI}}_2$ crystals. Usually the role of the intrinsic defect states for the different semiconductors is not appropriately considered due to the incorporation of the delocalized electrons predominantly forming the top of the valence band. Additionally, some disturbances of the energy band dispersion in k space and thus inaccuracies in the interpretation of experimental data are due to their electron-phonon broadening as well as resonance exciton contribution¹¹.

There are many chalcogenide crystals starting from binary system up to quaternary ones. Some of them possess crystal structure but more of them are solid state alloys¹². All of the mentioned systems, even crystalline chalcogenides, are plenty of intrinsic point defects of different origin¹³. This fact is usually neglected during theoretical study and calculations but the role of defects may be very crucial. The structural imperfections give irrefutable contribution to the band structure and optical character of material principally different to the perfect crystals features¹⁴. The defects form new trapping levels within the forbidden energy gap or additional bands of energy that designs material possessing improved quantum efficiency and can be used as perspective compounds for solar cells requiring high visible - near infrared absorption and substantial differences between the carrier mobility.

The defects and especially vacancies formations in binary system were studied theoretically in many works¹⁵⁻¹⁹ but the imperfections occurring in the ternary system were studied theoretically less frequently²⁰⁻²². Moreover, most of the tested materials are oxides including neutral oxygen vacancies. However, the manifestation of the optical and transport properties with defects taking into account remain not clear to the end²³. To the best of our knowledge, the quaternary crystals were not investigated according to the structure imperfections and their influence at the optical properties. Most of the existed theoretical works are devoted to the structural and electronic properties investigations of perfect crystalline quaternary chalcogenides applying different density functional theory (DFT) potentials²⁴⁻²⁸. Also the influence of the compounds content on the electronic properties of quaternary alloys was studied²⁹. Recently, great efforts on exploring quaternary chalcogenides have discovered many novel NLO crystals and some of them were also analyzed theoretically^{6,30}.

Unfortunately, there are no theoretical reports in the literature concerning research on the $\text{Ag}_2\text{In}_2\text{GeSe}_6$ and $\text{Ag}_2\text{In}_2\text{SiSe}_6$ crystals. Hence, to provide a basis for understanding the future concept of devices, their design and applications, we have determined the structural and electronic properties of the mentioned chalcogenides applying the plane-wave norm-conserving pseudopotential approach within DFT

Table 1 Lattice parameters of $\text{Ag}_2\text{In}_2\text{SiSe}_6$ and $\text{Ag}_2\text{In}_2\text{GeSe}_6$ crystal structures

Parameters	$\text{Ag}_2\text{In}_2\text{SiSe}_6$ ⁴	$\text{Ag}_2\text{In}_2\text{GeSe}_6$ ³
Space group	monoclinic space group Cc	monoclinic space group Cc
a [nm]	1.26683(4)	1.2692(3)
b [nm]	0.74565(3)	0.7492(1)
c [nm]	1.26133(4)	1.2644(3)
β [°]	109.286(2)	109.50(3)

formalism. First, the lattice parameters and electronic band gap of both crystals have been modelled. Second, the electronic properties of defected structures were studied.

Computational details

Crystal structure of $\text{Ag}_2\text{In}_2\text{SiSe}_6$ and $\text{Ag}_2\text{In}_2\text{GeSe}_6$

$\text{Ag}_2\text{In}_2\text{SiSe}_6$ and $\text{Ag}_2\text{In}_2\text{GeSe}_6$ crystals possess monoclinic space group C_c (point group number 9). Their crystal parameters as well as the atomic positions were studied in the works of Olekseyuk et al.⁴ and Krykhovets et al.³. In the Table 1 the experimentally obtained lattice parameters of the mentioned crystals are presented. The investigated structures differ only by a type of IV row atoms (C^{IV}). The unit cell of $\text{Ag}_2\text{In}_2\text{GeSe}_6$ structure is a little bit bigger than the one of $\text{Ag}_2\text{In}_2\text{SiSe}_6$. It is due to the radius of Si and Ge. The crystal radius of Si and Ge are equal to 1.11 Å and 1.25 Å, respectively³¹. In Table 2 the fractional positions for all representative atoms of both structures are collected following the work of Olekseyuk et al.⁴ and Krykhovets et al.³. These atom positions were used as starting values for the computer simulations of the electron band structures for the investigated chalcogenides.

Details of the band structure calculations

To study the structural, electronic and spectral features of perfect and defective $\text{Ag}_2\text{In}_2\text{SiSe}_6$ and $\text{Ag}_2\text{In}_2\text{GeSe}_6$ crystals the DFT methodology was used. For all performed computational steps the Cambridge serial total energy package (CASTEP)

Table 2 Atomic fractional coordinates of $\text{Ag}_2\text{In}_2\text{SiSe}_6$ and $\text{Ag}_2\text{In}_2\text{GeSe}_6$ crystal structures

Atoms name	$\text{Ag}_2\text{In}_2\text{SiSe}_6$			Atoms name	$\text{Ag}_2\text{In}_2\text{GeSe}_6$		
	x/a	y/b	z/c		x/a	y/b	z/c
Ag1	0.3978(8)	0.5899(7)	0.2528(7)	Ag1	0.3909(2)	0.5890(3)	0.2570(2)
Ag2	0.6005(8)	0.2042(6)	0.4148(7)	Ag2	0.5936(2)	0.2053(3)	0.4167(2)
In1	0.4179(7)	0.0945(6)	0.0615(7)	In1	0.4114(1)	0.0920(2)	0.0641(1)
In2	0.2333(7)	0.0587(5)	0.2576(6)	In2	0.2308(1)	0.0632(2)	0.2625(1)
Si1	0.162(2)	0.763(2)	0.001(2)	Ge	0.1634(2)	-0.2355(3)	0.0053(2)
Se1	0.35600	0.7532(8)	0.05100	Se1	0.3556(2)	-0.2465(3)	0.0510(2)
Se2	0.4050(9)	0.2353(8)	0.2460(8)	Se2	0.4000(2)	0.2361(3)	0.2464(2)
Se3	0.0956(9)	0.0090(1)	0.0563(7)	Se3	0.0850(2)	0.0089(3)	0.0628(2)
Se4	0.0982(9)	0.2690(8)	0.3115(9)	Se4	0.0875(2)	0.2661(3)	0.3123(2)
Se5	0.2882(9)	0.2379(7)	0.8703(8)	Se5	0.2834(2)	0.2300(3)	-0.1230(2)
Se6	0.6283(8)	0.0185(8)	0.0901(7)	Se6	0.6163(2)	0.0136(3)	0.0898(2)

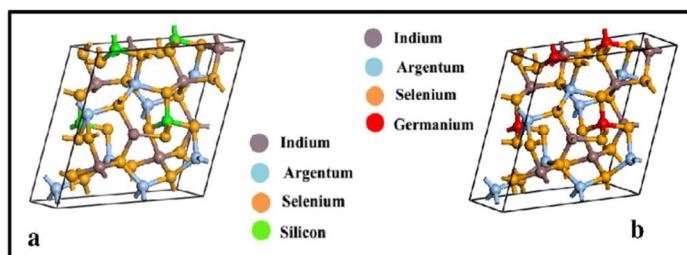


Fig. 1 The unit cell of $\text{Ag}_2\text{In}_2\text{SiSe}_6$ (a) and $\text{Ag}_2\text{In}_2\text{GeSe}_6$ (b) structures

program³², containing the Materials Studio program module, was applied. The CASTEP program is based on total energy plane-wave pseudopotential method. The initial structural data of the investigated structures were implemented as it is presented in Table 1 and 2. The such formed unit cells for the both structures are shown in Figure 1.

First of all the geometries for the both investigated structures were optimised with respect to the total energy minimization applying the Broyden-Fletcher-Goldfarb-Shanno (BFGS) algorithm³³. The size of the unit cells and the symmetry of crystals were conserved during the geometry optimisation procedure. This is due to the need to preserve the crystallinity of investigated structures. The convergence criteria for optimization were chosen as follow: the convergence of total energy during geometry optimization procedure was equal to $2 \cdot 10^{-5}$ eV/atom, force on the atom was less than 0.01 eV/Å, the stress on the atom was not more than 0.02 GPa, the maximal atomic displacement was equal to $5 \cdot 10^{-4}$ Å. The electronic exchange-correlation energy was treated within the frame of the generalized gradient approximation (GGA) using Perdew-Burke-Ernzerhof (PBE)³⁴ and the B3LYP^{35,36} potentials. In order to allow performance of calculations with the lowest possible cut-off energy for the plane-wave basis set, norm-conserving pseudopotentials have been used in the calculations³⁷. Pseudoatomic calculations were performed for Ag 4s2 4p6 4d10 5s1, In 5s2 5p1, Si 3s2 3p2, Se 4s2 4p4 configurations. The cut-off energy of the plane-wave basis set was chosen equal to 650 eV. The special points numerical sampling integration over the Brillouin zone were carried out using the Monkhorst-Pack method with the $3 \times 5 \times 3$ special k -point mesh. The total energy was assumed to be converged when the self-consistent field (SCF) tolerance reached the value 10^{-5} eV/atom. The calculations were performed for a primitive unit cell of the $\text{Ag}_2\text{In}_2\text{SiSe}_6$ and $\text{Ag}_2\text{In}_2\text{GeSe}_6$ crystal structures.

The electronic band structure and optical features were computed for optimised structure using GGA/PBE and GGA/B3LYP functionals. The computational and convergence parameters for the energy calculations were applied as presented above for geometry optimization procedure.

Table 3 Identification of silver and indium interchanged defects in $\text{Ag}_2\text{In}_2\text{SiSe}_6$ and $\text{Ag}_2\text{In}_2\text{GeSe}_6$ crystals

Structure	Position of atoms	Defect identification
Crystal structure	Ag1 Ag2 In1 In2	
Defected structure (1)	In1 Ag2 Ag1 In2	D1
Defected structure (2)	Ag1 In2 In1 Ag2	D2
Defected structure (3)	In1 In2 Ag1 Ag2	D3

Defects and vacancies

In semiconductors, lattice point defects such as vacancies can act as very efficient localized trapping levels for electrons, holes and excitons, and may strongly influence on transport and optical properties of the host material. The DFT calculations become an indispensable tool for studying the electronic properties caused by defects. Applying the computational methodology described in the previous sub-paragraph the defected $\text{Ag}_2\text{In}_2\text{SiSe}_6$ and $\text{Ag}_2\text{In}_2\text{GeSe}_6$ crystals were simulated.

The two kind of defective systems were studied. In the first one the silver and indium atoms were interchanged, and in the second one the silver, indium, selenium or respectively, silicon and germanium neutral vacancies were built. The geometries of all defected crystals were optimized with the parameters specified in the previous section applying the DFT/PBE potential. In this case, the lattice parameters and the position of atoms were fluctuated.

In the Table 3 the identification of defects are specified. The defect D1 was created by interchanging the position of the In1 and Ag1 atoms. The defect D2 is the interchanging of In2 and Ag2 atoms positions and the defect D3 characterize the two mentioned interchanges at the same moment. The selenium vacancies are indicated by Se1 up to Se6 for both $\text{Ag}_2\text{In}_2\text{SiSe}_6$ and $\text{Ag}_2\text{In}_2\text{GeSe}_6$ structures. The symbol Se1 means that the selenium atom named Se1 (defined in Table 2) was removed from the structure. In the investigated chalcogenide crystal structures the cation vacancies were created by removing from the structure Ag, In and Si or Ge, respectively. These vacancies were indicated as Ag1, Ag2, In1, In2, Si, Ge when the defined in Table 2 atom is removed from the perfect crystal structure.

The discussion of the defect formation energies and the electronic and optical properties of the defected structures will be presented in the following parts of the presented work.

Results and discussion

Crystal structure of $\text{Ag}_2\text{In}_2\text{SiSe}_6$ and $\text{Ag}_2\text{In}_2\text{GeSe}_6$

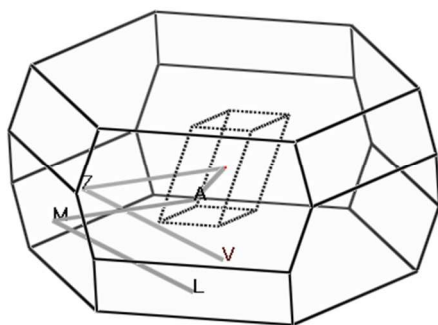


Fig. 3 The Brillouin zone for a primitive cell of investigated crystals

The theoretical investigations of electronic properties and optical features for the two selected chalcogenide crystals are the main aim of the presented work. To achieve the specified goal the electronic band structures of the $\text{Ag}_2\text{In}_2\text{SiSe}_6$ and $\text{Ag}_2\text{In}_2\text{GeSe}_6$ single crystals were calculated applying DFT/PBE and DFT/B3LYP potentials. First of all the geometry of the two mentioned systems was optimised preserving the symmetry of the crystals and the lattice parameters. It means that the size of the unit cell did not evaluate and the point group was fixed as C_c . The experimentally measured inter-atomic distances and the data obtained theoretically after geometry optimisation are presented in Table 4. Following these results one can see that the Ge-Se bonds are longer with respect to the Si-Se bonds. It is due the fact that the Ge atom radius is 0.14 Å higher than the radius of Si even if the ionic radii of Ge^{+4} and Si^{+4} are equal to 0.039 nm and 0.040 nm, respectively. In addition, all the

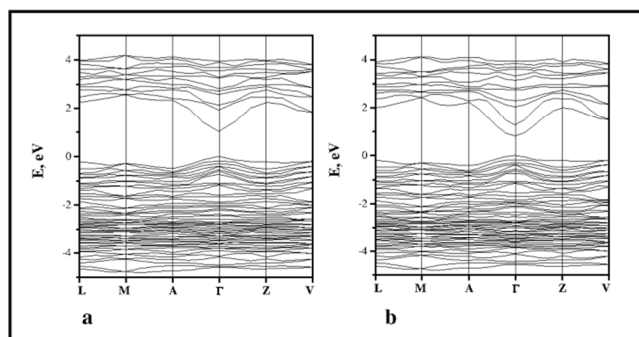


Fig. 2 Calculated band structure of $\text{Ag}_2\text{In}_2\text{SiSe}_6$ (a) and $\text{Ag}_2\text{In}_2\text{GeSe}_6$ single crystals (b) using DFT/PBE potential

cationic-anionic bonds tend to be more tetrahedral. After geometry optimization the Ag-Se bonds are generally longer than those obtained from experiment but the In-Se bonds are going to be shorter than in the case of the starting geometry. For both crystals the In-Se bonds are shorter than the Ag-Se ones. The optimised and experimentally obtained bond lengths differ one from other not more than 3 %.

For such optimised crystal structures their electronic properties were calculated. The band structure calculations were performed in k space within the Brillouin zone (BZ) directions shown in Figure 2. The coordinates of the special points of the BZ are (in units of the reciprocal lattice vectors) L $(-1/2, 0, 1/2)$; M $(-1/2, -1/2, 1/2)$; A $(-1/2, 0, 0)$; Γ $(0, 0, 0)$; Z $(0, -1/2, 1/2)$, V $(0, 0, 1/2)$. In the Figure 3 the calculated band structures for both investigated crystals are presented. The Figure 3a and 3b presents the energy band structure computed

Table 4 Inter-atomic distances in $\text{Ag}_2\text{In}_2\text{SiSe}_6$ and $\text{Ag}_2\text{In}_2\text{GeSe}_6$ single crystals

Bond identification	Bond length			
	$\text{Ag}_2\text{In}_2\text{SiSe}_6$		$\text{Ag}_2\text{In}_2\text{GeSe}_6$	
	Exp ⁴ [nm]	DFT/PBE [nm]	Exp ³ [nm]	DFT/PBE [nm]
Ag1-Se1	0.2711	0.274496	0.2780(4)	0.276582
Ag1-Se2	0.2648(8)	0.266620	0.2652(3)	0.276341
Ag1-Se4	0.2745(15)	0.270416	0.2704(4)	0.270699
Ag1-Se5	0.2671(14)	0.272499	0.2717(4)	0.273275
Ag2-Se2	0.2690(14)	0.269275	0.2682(4)	0.269380
Ag2-Se3	0.2799(11)	0.282534	0.2854(4)	0.282664
Ag2-Se5	0.2652(15)	0.268887	0.2664(5)	0.270172
Ag2-Se6	0.2693(10)	0.267130	0.2673(4)	0.267942
In1-Se1	0.2654	0.254664	0.2623(3)	0.254268
In1-Se2	0.2607(13)	0.254939	0.2592(4)	0.254805
In1-Se5	0.2654(13)	0.254435	0.2595(4)	0.255016
In1-Se6	0.2631(14)	0.254332	0.2579(4)	0.253669
In2-Se2	0.2588(14)	0.255183	0.2574(4)	0.254906
In2-Se3	0.2588(12)	0.254757	0.2616(4)	0.254483
In2-Se4	0.2573(13)	0.252890	0.2604(4)	0.252688
In2-Se5	0.2597(9)	0.253565	0.2593(3)	0.254344
Si / Ge-Se1	0.2330	0.226638	0.2313(5)	0.234140
Si / Ge-Se3	0.222(2)	0.225268	0.2314(4)	0.233001
Si / Ge-Se4	0.227(3)	0.225843	0.2316(4)	0.233850
Si / Ge-Se6	0.225(2)	0.228132	0.2336(4)	0.235657

Table 5 Effective mass of electrons and holes calculated by DFT/PBE potential for different structures in two perpendicular directions of the Brillouin zone

Structure	Effective mass of electrons		Effective mass of holes	
	$m_e^* \parallel a$	$m_e^* \perp a$	$m_h^* \parallel a$	$m_h^* \perp a$
Ag ₂ In ₂ SiSe ₆	0.1944 m_e	0.1449 m_e	0.5372 m_e	0.4015 m_e
Ag ₂ In ₂ GeSe ₆	0.4066 m_e	0.2494 m_e	0.8894 m_e	0.5320 m_e
Ag ₂ In ₂ SiSe ₆ + Se6	0.2014 m_e	0.5008 m_e	2.0568 m_e	0.5045 m_e
Ag ₂ In ₂ GeSe ₆ + Se6	0.1917 m_e	0.7569 m_e	2.7155 m_e	0.7829 m_e
Ag ₂ In ₂ SiSe ₆ + AgI	0.7007 m_e	0.1899 m_e	3.2632 m_e	2.2294 m_e
Ag ₂ In ₂ GeSe ₆ + AgI	0.1562 m_e	0.5999 m_e	4.0005 m_e	1.5914 m_e

for the Ag₂In₂SiSe₆ and Ag₂In₂GeSe₆ crystals, respectively using DFT/PBE functional. The both crystals are direct band gap semiconductors. It is typical to other Se chalcogenide compounds³⁸. The top of the valence band and the bottom of the conduction band are located at the centre of the BZ (Γ point). It is similar to the other quaternary crystals³⁹. The DFT/PBE potential gives the energy gap equal to 1.02 eV and 0.81 eV for the Ag₂In₂SiSe₆ and Ag₂In₂GeSe₆ crystals, respectively. The energy band calculated by DFT/B3LYP potential has the same dispersion as those computed by DFT/PBE functional though, the conducting band calculated by DFT/B3LYP is shifted towards the higher energies for the both crystals and gives to high value. It is well-known that, the band gap magnitude is almost always underestimated within a framework of DFT calculations approach³⁸, therefore the DFT/B3LYP functional approach gives the worst results comparing to the experimental data and only the DFT/PBE approach for the further research will be used.

Analyzing the Figures 3a and 3b one can see that the shape of energy curves creating the valence bands possess dispersion prevailingly near the centre of the BZ which reflects the contribution of the long-range potential formed predominantly by the p-originating states. The points farther off the Γ point of the BZ are less sensitive to the delocalization. The more significant dispersion of the energy in the k -space possesses the bottom of conducting band reflecting the higher mobility of the corresponding electrons. It is prevailingly observed for both investigated crystals following the A - Γ - Z direction and it correlates sufficiently well to the general crystallochemistry image. The high anisotropy of the holes mobility (top of the valence band) and the one of electrons (bottom of the conduction band) may be promising to use of such crystals in the LED and photovoltaic devices because it allows to achieve the charge separation in the desired points between the electrodes. Additionally such behaviour may be used for the formation of the different heterojunctions where the coexistence of the carriers (holes and electrons) with different motilities is necessary to operate by their diffusion lengths and annihilation near the electrodes.

From the fundamental solid state point of view the calculated dispersion of the band structure is principal for calculation of the carriers effective masses. The effective mass of electrons (m_e^*) was evaluated from the curvature (energy derivatives) of the bottom of conduction band in k space. The diagonal elements of the effective mass tensor for electrons and holes are calculated around Γ point of BZ for conduction and valence band, respectively, following the equation:

$$\frac{1}{m_{eij}^*} = \frac{1}{\hbar^2} \frac{\partial^2 E(k)}{\partial k_i \partial k_j} \quad (1)$$

The effective mass of electron is determined by fitting the conducting band structure to a parabolic function. The electron effective mass for Ag₂In₂SiSe₆ structure is lower with respect to Ag₂In₂GeSe₆ what reflect a fact that the parabolic curvature of Ag₂In₂SiSe₆ is greater than that of Ag₂In₂GeSe₆ confirming a statement that the effective mass is inversely proportional to the band energy curvatures. The calculated electron effective mass ratio to the free electron (m_e^*/m_e) for Ag₂In₂SiSe₆ and Ag₂In₂GeSe₆ crystals is equal to 0.1449 and 0.2494 ($m_e^* \perp a$), respectively. So despite the similarity of computed energy gaps presented value of the m_e^*/m_e ratio is almost two times different and the replacement of the Ge by Si leads to almost two times enhancement of the anisotropy. The electron mobility in direction parallel to the a axes of unit cell is lower than in perpendicular direction (see Table 5) confirming the substantial anisotropy. Generally, the more significant anisotropy for the Ag₂In₂GeSe₆ crystal with respect to the Ag₂In₂SiSe₆ have been established. It is also observed for the hole mobility. The effective mass of holes is predicted from the band dispersion curvature of the valence band maximum and is equal to 0.4015 and 0.5320 ($m_e^* \perp a$) as well as 0.5372 and 0.8894 ($m_e^* \parallel a$) for the Ag₂In₂SiSe₆ and Ag₂In₂GeSe₆ crystals, respectively. So again there exists a huge anisotropy. It is necessary to emphasize that these parameters are evaluated with neglecting of an electron-phonon interaction causing the energy band broadening which is particularly strong in the chalcogenide compounds.

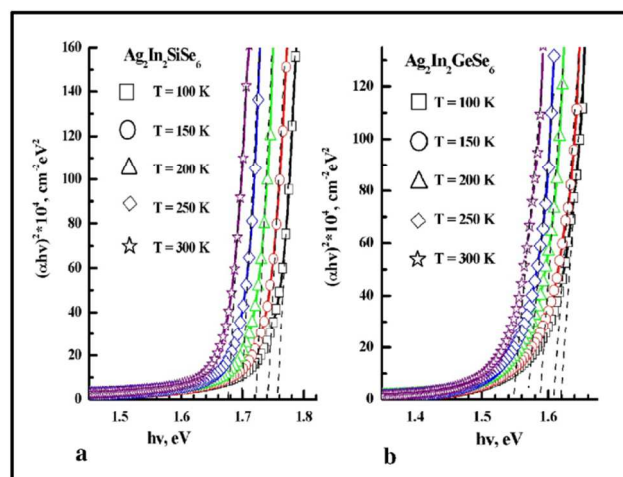


Fig. 4 Experimental spectral dependence of absorption coefficient versus temperature (non-polarized) for the $\text{Ag}_2\text{In}_2\text{GeSe}_6$ (a) and $\text{Ag}_2\text{In}_2\text{SiSe}_6$ (b) crystals

Figure 4 shows the optical absorption spectra for the $\text{Ag}_2\text{In}_2\text{SiSe}_6$ and $\text{Ag}_2\text{In}_2\text{GeSe}_6$ single crystals versus temperature. Band gap's magnitudes were fitted graphically using a Tauc plot⁴⁰ by scheming $(\alpha \cdot hv)^n$ vs hv and using the x-axis intercept of a linear fit to the Tauc plot. The value of the exponent, n , indicates the type of involved transition: $n = 1/2$ indicates an indirect band transition, and $n = 2$ indicates a direct band transition⁴¹. It is in agreement to the theoretically computed energy band structure presented in Figure 3a and 3b where for both structures direct energy gap is established. In the Figure 4 one may see that the optical band gap decreases with increasing temperature for the both crystals. It is typical for the semiconducting materials. The absorption coefficient increases sharply above 1.55 eV for $\text{Ag}_2\text{In}_2\text{GeSe}_6$ and above 1.68 eV for $\text{Ag}_2\text{In}_2\text{SiSe}_6$ at ambient temperature (300 K). For the lower temperature (100 K) these values are equal to 1.62 eV and 1.76 eV, respectively. From the Figure 5 (left panel) one can see that the theoretically obtained results are in qualitative agreement to the experimental data even without taking into account the contribution of the phonon subsystem. So one can expect that for this specific case the role of the phonon subsystem is not crucial. Energy gap obtained for the $\text{Ag}_2\text{In}_2\text{SiSe}_6$ is higher than the magnitude obtained for $\text{Ag}_2\text{In}_2\text{GeSe}_6$ crystal. The band gaps of the investigated crystals are larger than the corresponding values for the AgInSe_2 where the energy gap is equal to 1.24 eV⁴². The SiSe_2 is a semiconductor with an indirect band gap $E_g = 1.73$ eV at room temperature^{43,44}. Germanium diselenide (GeSe_2) is a IV–VI chalcogenide semiconductor with a wide band gap of 2.70 eV⁴⁵. It seems that the adding of the SiSe_2 or GeSe_2 to the AgInSe_2 favours an enhanced energy gap of $\text{Ag}_2\text{In}_2\text{SiSe}_6$ as well as of $\text{Ag}_2\text{In}_2\text{GeSe}_6$.

Concluding one may say that the theoretically obtained absorption spectra for both crystals are in qualitative agreement to the experimental data. Generally one may say that the DFT methodology specially the pure GGA/PBE potential underestimate the energy gap and thus shifts the absorption edge towards lower energies (so called red shift). The hybrid

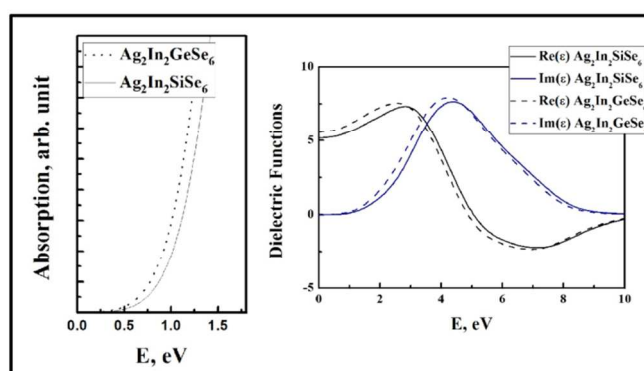


Fig. 5 The theoretically calculated absorption spectra (left panel) and the dielectric functions (right panel) for the $\text{Ag}_2\text{In}_2\text{SiSe}_6$ and $\text{Ag}_2\text{In}_2\text{GeSe}_6$ crystal structures using DFT/PBE approach

potential B3LYP gives exactly the same shape of absorption curve but the results are overestimated. The B3LYP potential is formed by 20 % of Hartree-Fock exchange potential and maybe it is too strong to reproduce quantitatively the energy gap value. The investigated crystals are characterized prevalingly by covalent bonds and this kind of material probably should be analyzed using long range correlated potential with small separation parameter⁴⁶ which will spreads the electron interaction.

In the Figure 5 (right panel) the calculated dispersion of real and imaginary parts of the dielectric function for both $\text{Ag}_2\text{In}_2\text{SiSe}_6$ and $\text{Ag}_2\text{In}_2\text{GeSe}_6$ crystal is presented. The black curves characterise the parameters for $\text{Ag}_2\text{In}_2\text{SiSe}_6$ structure and the blue ones are depicted for $\text{Ag}_2\text{In}_2\text{GeSe}_6$ crystal. Taking the square root from the values of $\text{Re}(\epsilon(\omega))$ in the limit of zero energy the refractive indices may be evaluated. For the $\text{Ag}_2\text{In}_2\text{SiSe}_6$ the mentioned value is equal to 2.75 and for $\text{Ag}_2\text{In}_2\text{GeSe}_6$ the refractive index is 2.37.

The Figures 6 and 7 show the partial electron density of states (DOS) diagrams calculated by the DFT/PBE methodology for $\text{Ag}_2\text{In}_2\text{SiSe}_6$ and $\text{Ag}_2\text{In}_2\text{GeSe}_6$ crystals, respectively. The presented DOS allow to analyse the atomic orbitals composition forming valence and conduction bands. The top of valence band of $\text{Ag}_2\text{In}_2\text{SiSe}_6$ is originated mainly from Se 4p and Ag 4d orbitals. The conduction band of mentioned material is formed mainly from the Se 4s state. Following the Figure 6 is obvious that the Se 4s states form additional energy level creating the bottom of conduction band. It is also seen in Figure 3a as the much lowered energy level at Γ point. The top of the valence band in the $\text{Ag}_2\text{In}_2\text{GeSe}_6$ crystal is very similar to the such for the $\text{Ag}_2\text{In}_2\text{SiSe}_6$. Also the top of valence band is originated mainly from the hybridized Se 4p - Ag 4d states possessing substantially degree of ionicity. The bottom of conduction band is created by admixture of Se 4s and Ge 4s terms. For the both structures the p chalcogen atom states are dominating in the valence band as seen in Figure 6 and 7. This may have serious implications on the band structure near the Fermi level. Also the conduction band minimum (CBM) is composed by the chalcogen atoms states.

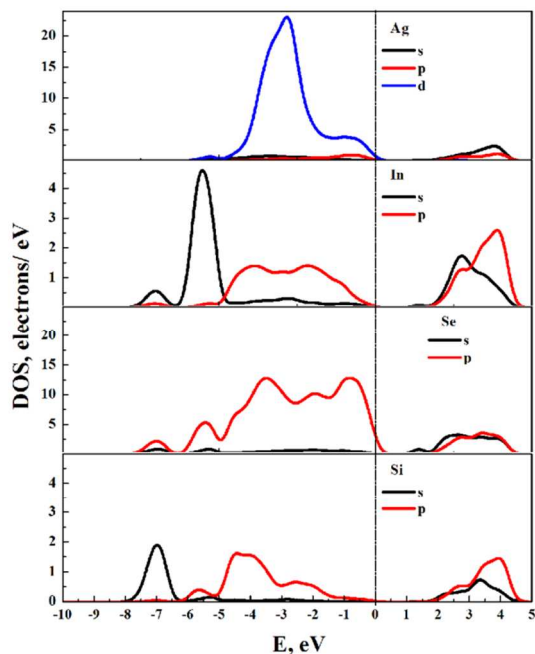


Fig. 6 Density of states (DOS) diagrams calculated for $\text{Ag}_2\text{In}_2\text{SiSe}_6$ by DFT/PBE

The Figure 8 presents the electron density calculated by DFT/PBE potential for the $\text{Ag}_2\text{In}_2\text{SiSe}_6$ structure projected in the plane of Si atoms. One can see that evident electron density is observed near the Ag and Se atoms. The space charge overlap between the Ag and Se atoms confirms the covalent character of the bonds between them. It is typical for the chalcogenide structures.

Band structures of $\text{Ag}_2\text{In}_2\text{SiSe}_6$ and $\text{Ag}_2\text{In}_2\text{GeSe}_6$ with defects taking into account

One of the most important parameter that can be evaluated from first-principles calculations is the defect formation energy. It gives an information on the overall stability of a created intrinsic defect as well as the relative stabilities between different atomic configurations and charge states. The

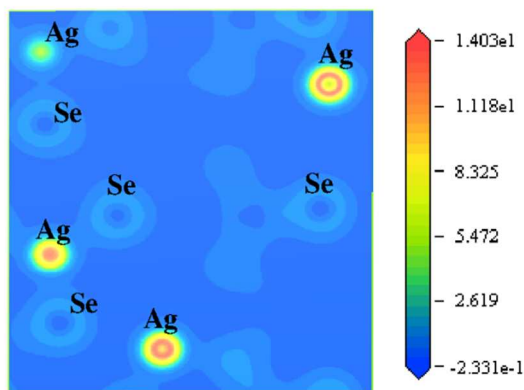


Fig. 8 Electron density calculated by DFT/PBE potential for the $\text{Ag}_2\text{In}_2\text{SiSe}_6$ projected in the plane of Si atoms

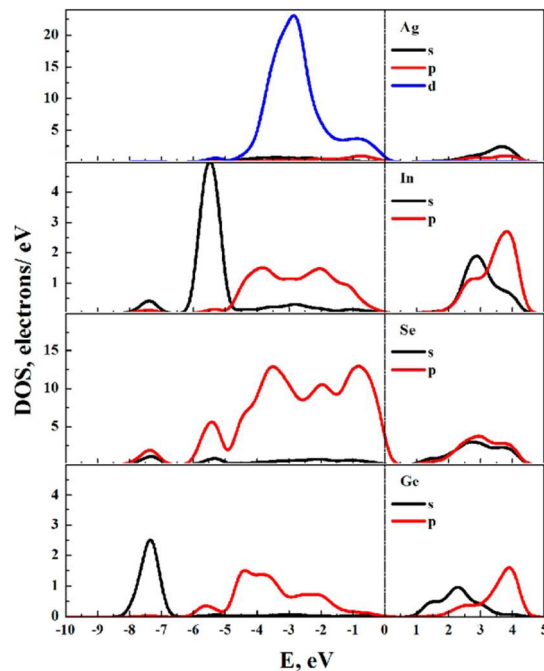


Fig. 7 Density of states (DOS) diagrams calculated for $\text{Ag}_2\text{In}_2\text{SiSe}_6$ by DFT/PBE

formation energy E_f of a neutral vacancy is the Gibbs free energy and can be defined as⁴⁷:

$$E_f = E_{def} - E_{exact} + \sum_{i=1}^n \mu_i - T\Delta S_f + P\Delta V_f \quad (2)$$

Where E_{def} and E_{exact} are the total energy of the super cell with a neutral vacancy and the total energy of the perfect super cell, respectively. The μ_i denotes the chemical potential of corresponding atom escaped from the perfect system. The ΔS_f is the change in vibrational entropy, and ΔV_f is the variation of volume when the defect is incorporated into the system. Since the contribution of volume changes is relatively small and the changes in entropy are of the same order compared to different defects, one can focus on the first three expressions of Equation 2. The two last terms in mentioned equation can be neglected for the solid phase⁴⁸. The defect formation energy has an influence on the concentration of a point defect via $C = Ne^{-E_f/k_B T}$ under thermodynamic equilibrium conditions. The N is the lattice point density, k_B is the Boltzmann constant, and T is the absolute temperature.

Computing the defects formation possibility for all the investigated structures first of all their geometry was optimised. The internal relaxations play a significant role in computing of adequate formation energies¹⁵. In the Figure 9 the D1, D2 and D3 defects formation energies for the $\text{Ag}_2\text{In}_2\text{SiSe}_6$ and $\text{Ag}_2\text{In}_2\text{GeSe}_6$ crystals are presented. One can see that the defect formation energies for both structures are similar except the energy of D3 defect in $\text{Ag}_2\text{In}_2\text{SiSe}_6$ crystal. This system has the lowest stability and also the mentioned defect affect the most drastic changes in the electronic properties of the system. The value of energy gap for the $\text{Ag}_2\text{In}_2\text{SiSe}_6/\text{D3}$ structure decreases up to 0.29 eV. The energy bands dispersion versus the direction of BZ for all the defected structures possess the same feature as it is observed for the perfect crystal structure (see Figure 3a and

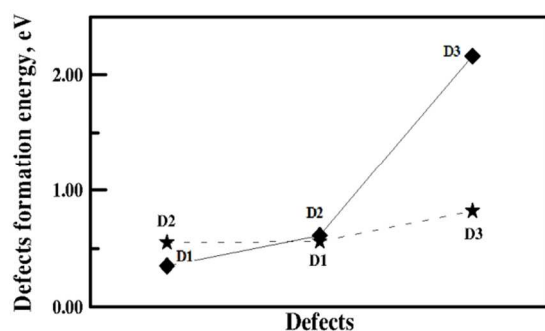


Fig. 9 The D1, D2 and D3 defects creation energy for Ag₂In₂SiSe₆ (solid line) and Ag₂In₂GeSe₆ (dashed line).

3b). The mentioned defects shift the conducting bands to the lower energy decreasing energy gap. Although, in this case any additional energy bands are observed for the calculated energy band structure. Any of the D1, D2 and D3 defects does not give significant contribution to the electronic and optical properties of Ag₂In₂SiSe₆ and Ag₂In₂GeSe₆ structures creating additional traps for charge carriers. Also the absorption band for defected structures has the spectral dependence similar to the presented in Figure 5a and is red shifted.

The selenium vacancies in Ag₂In₂SiSe₆ and Ag₂In₂GeSe₆ crystals were also investigated. The selenium atoms in studied structures have anion character but to keep the system not charged the neutral vacancies were formed. The selenium vacancies formation energy for both structures is significantly higher than activation energy of D defects (compare Figure 9 and 10). The S1÷S6 vacancies created in Ag₂In₂SiSe₆ need the similar formation energy changing from 10.13 eV up to 10.83 eV. However, the existing selenium vacancies in Ag₂In₂GeSe₆ structure need energy varying within the 9.29 - 12.19 eV. The origin of the six of selenium vacancies is different because these atoms possess different coordination. For both structures the vacancies S2 and S5 have higher formation energies than the other three vacancies due to connectivity between selenium atoms and their neighbours. The selenium atoms numbered as 2 and 5 have four neighbouring atoms in first coordination sphere. The other selenium atoms have three adjacent atoms and all of them in contrary to the 2 and 5 selenium are connected to the Si or Ge atoms, respectively. These facts cause the S2 and S5 vacancies formation energy higher than the formation energy of vacancies S1, S3, S4 and S6. The vacancy S6 has the same formation energy equal to 10.43 eV, for the both Ag₂In₂SiSe₆ and Ag₂In₂GeSe₆ structure. Additionally only the S6 vacancy gives a reduction of energy gap for the both crystals.

The introduction of point defects would unavoidably change the band structure of the perfect crystal. Generally speaking, point defects can introduce new defects associated energy states intra the forbidden band gap, or introduce resonant states in the valence bands or conduction bands area¹⁸. For a sufficiently large supercell, the VBM and CBM may be nearly not disturbed by the defect states or resonant states. In the performed calculations the presence of the defect in each unit

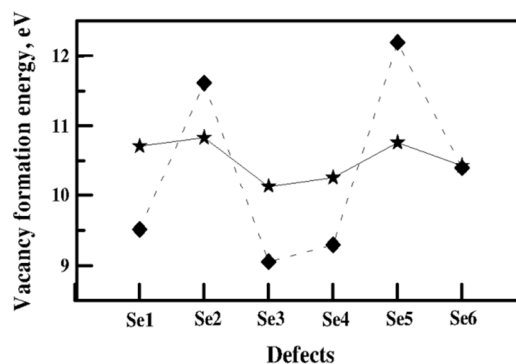


Fig. 10 The Se1, ..., Se6 vacancies formation energy for Ag₂In₂SiSe₆ (solid line) and Ag₂In₂GeSe₆ (dashed line).

cell is considered. It should have obvious influence on the energy band structure of defected crystals. Normally their concentration is substantially less. The energy band structure computed for Ag₂In₂SiSe₆ and Ag₂In₂GeSe₆ crystals possessing Se6 vacancies is shown in the Figure 11. One can conclude that compared to the discussed before perfect crystal structure the vacancy Se6 gives additional energy level near the bottom of conduction band. The valence band has the same shape for both Se6 defected as well as perfect crystals. The top of the valence band for the Ag₂In₂SiSe₆ and Ag₂In₂GeSe₆ structure with Se6 vacancy is originated from Se 4p and Ag 4d states. The bottom of the conduction band is formed by hybridization of In 4p, Se 4p and Si 3p or Ge 4p orbitals, respectively (see Figure 12). In the energy gap region additional band is created due to the hybridization of the mentioned orbitals. It is observed for the both structures. The influence of Ge atom on the electronic properties of investigated Se6 vacancy reached structures is indicated in the energy gap reduction compared to the role of Si. The observed changes in DOS and calculated energy band may give an impression that significant changes in optical properties of studied structures also will be seen, but

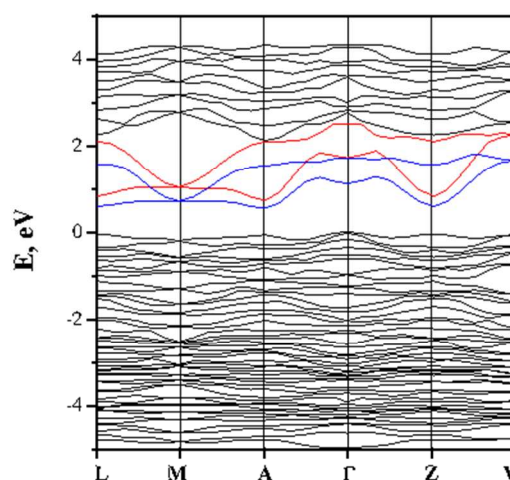


Fig. 11 The band structure of Se6 vacancies possessing structures: red bands belong to Ag₂In₂SiSe₆ and the blue ones to Ag₂In₂GeSe₆. The black bands are common for both structures

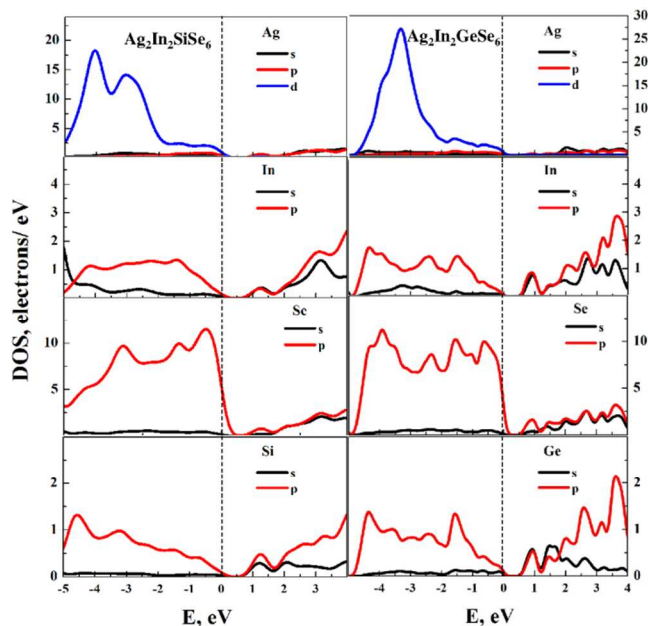


Fig. 12 DOS diagrams of $\text{Ag}_2\text{In}_2\text{SiSe}_6$ and $\text{Ag}_2\text{In}_2\text{GeSe}_6$ possessing Se_6 vacancy calculated by DFT/PBE potential

unfortunately the calculated absorption spectra look exactly like it was obtained for perfect crystal. The structure defected by Se_6 vacancies is a semiconducting material with indirect energy gap and the energy bands formed at the bottom of conduction band are not manifested in the experimental UV-VIS absorption. The transition from VBM to CBM is forbidden.

Analyzing the Figure 11 one may see that the VBM is located at the Γ point of the BZ and the CBM is at the A point for both the $\text{Ag}_2\text{In}_2\text{SiSe}_6$ and the $\text{Ag}_2\text{In}_2\text{GeSe}_6$ crystals. The band energy dispersion is similar for the both compounds. Following the presence of the band energy dispersion in the defect induced CBM one can say that the electron mobility has significant anisotropy. The mobility of electrons in $\text{Ag}_2\text{In}_2\text{GeSe}_6$ crystals possessing the S_6 vacancy is very low in direction perpendicular to the a axes but the mobility of holes is low in the direction parallel to a . The same situation exists for the $\text{Ag}_2\text{In}_2\text{SiSe}_6$ defected structure. The mobility of holes (for both directions) in the case of both S_6 defected structure is lower compare to the situation recorded for the perfect crystals (see Table 5). The mobility of electrons decreases in both directions for the $\text{Ag}_2\text{In}_2\text{SiSe}_6$ defected structure but the $\text{Ag}_2\text{In}_2\text{GeSe}_6$ defected structure favour the mobility of electrons in direction parallel to a . The carriers mobility for both crystals with structures reached in S_6 vacancies is significantly anisotropic. Theoretically it will favour the mentioned material for the photovoltaic applications.

Also the cationic vacancies were considered in the $\text{Ag}_2\text{In}_2\text{SiSe}_6$ and $\text{Ag}_2\text{In}_2\text{GeSe}_6$ crystals. These vacancies were created by removing the Ag1, Ag2, In1, In2 and Si or Ge atoms from crystal structure. First of all the geometries of the new defected structures were optimised allowing other atoms to change the position as well as relax supercell parameters. The vacancies formation energy is presented in the Figure 13. So

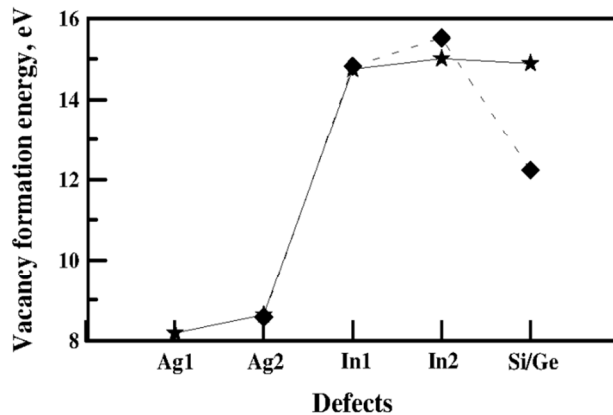


Fig. 13 The Ag1, Ag2, In1, In2 and Si or Ge vacancies formation energy for $\text{Ag}_2\text{In}_2\text{SiSe}_6$ (solid line) and $\text{Ag}_2\text{In}_2\text{GeSe}_6$ (dashed line)

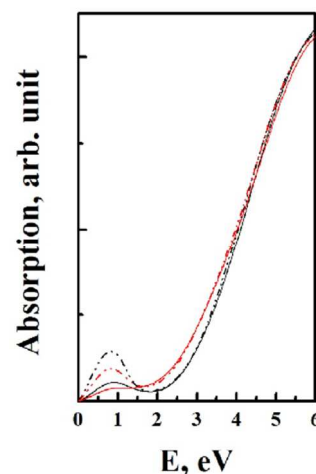


Fig. 14 The absorption spectra calculated by DFT/PBE methodology applied for $\text{Ag}_2\text{In}_2\text{SiSe}_6$ (black spectra) and $\text{Ag}_2\text{In}_2\text{GeSe}_6$ (red spectra) possessing Ag1 (solid line) and Ag2 (dashed line) vacancy

the vacancies named Ag1 and Ag2 have the same formation energy for both structures. Additionally the value of mentioned energy is relatively low and the probability of Ag1 and Ag2 vacancies forming is high. The UV-VIS absorption spectra of $\text{Ag}_2\text{In}_2\text{SiSe}_6$ structure possessing Ag1 and Ag2 cationic vacancies were calculated and the results are presented in Figure 14. There are clearly seen that Ag vacancies create additional absorption peak present for the excited state located between CBM and VBM of the perfect crystal structure. In the work of Tongay et al.⁴⁹ the existence of mentioned peak was associated to the defect existence but its character was not described. The intensity of the mentioned peak is higher for the $\text{Ag}_2\text{In}_2\text{SiSe}_6$ structure with respect to $\text{Ag}_2\text{In}_2\text{GeSe}_6$. It is in agreement with the experimentally obtained data presented in Figure 15. For the $\text{Ag}_2\text{In}_2\text{SiSe}_6$ structure small shoulder at the absorption edge band around 1.55 eV is evidently seen. This behaviour is not seen for the $\text{Ag}_2\text{In}_2\text{GeSe}_6$ crystal. It is due to the fact that the theoretically investigated structures are plenty of vacancies and their concentration is higher than it is observed in experiment. One can suppose that for higher

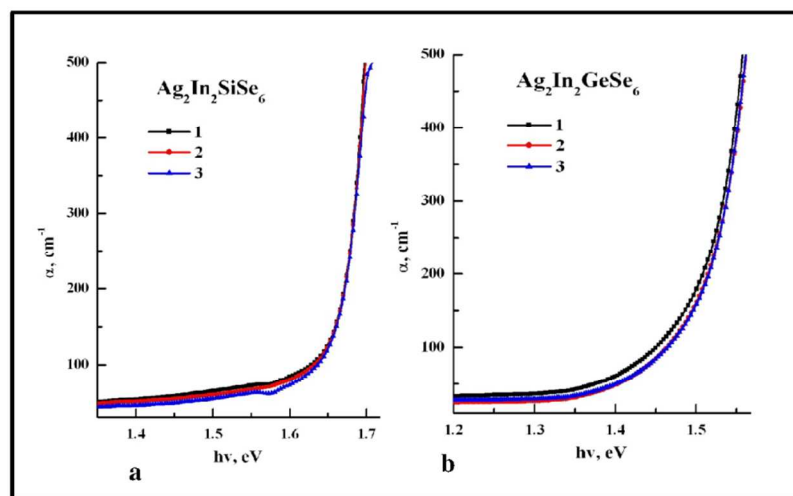


Fig. 15 Absorption edge for the $\text{Ag}_2\text{In}_2\text{SiSe}_6$ and $\text{Ag}_2\text{In}_2\text{GeSe}_6$ single crystal for different polarizations: 1 – non-polarized light; 2 – $E \parallel c$; 3 – $E \perp c$.

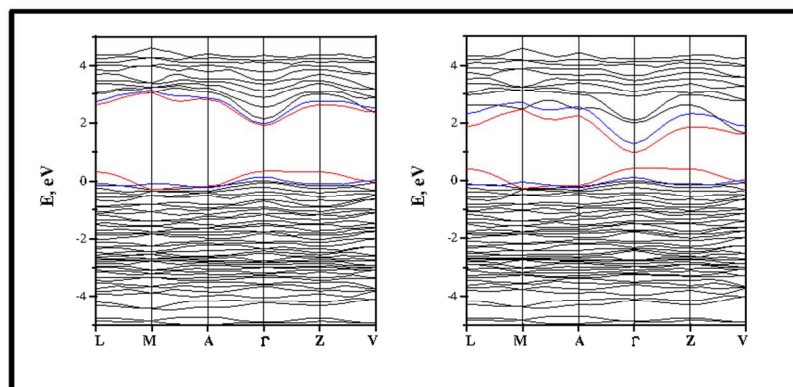


Fig. 16 The band structure for $\text{Ag}_2\text{In}_2\text{SiSe}_6$ (left panel) and $\text{Ag}_2\text{In}_2\text{GeSe}_6$ (right panel) possessing Ag1 (red bands) and Ag2 (blue bands) vacancies

concentration of Ag1 or Ag2 vacancies in experimentally investigated $\text{Ag}_2\text{In}_2\text{GeSe}_6$ the additional absorption peak may be also observed. The studied crystals may be considered like a promising materials for the simulations of the intrinsic cationic and anionic defects.

The Ag1 and Ag2 cation vacancies as point defects drastically modify the optical properties of investigated structures. It is caused by the new energy level created between CBM and VBM of perfect crystal. The Ag1 vacancies in both structures give the additional level above the valence band (Figure 16). The appearing localized energy levels introduced by the Ag1 vacancies are 0.34 eV and 0.43 eV above the VBM of perfect $\text{Ag}_2\text{In}_2\text{SiSe}_6$ and $\text{Ag}_2\text{In}_2\text{GeSe}_6$ crystals, respectively. These neutral Ag vacancies work like acceptor impurity in the investigated semiconductors and it is more pronounced for the Ag1 than for the Ag2 vacancy.

The Ag1 vacancies for both $\text{Ag}_2\text{In}_2\text{SiSe}_6$ and $\text{Ag}_2\text{In}_2\text{GeSe}_6$ structures have the lowest formation energy and due to the most probable existence of the mentioned defect the effective mass of electrons and holes was calculated. Analyzing the Figure 16

one may see that both structures are direct semiconducting materials with the VBM and CBM located at the Γ point of BZ. The mobility of electrons and holes in $\text{Ag}_2\text{In}_2\text{SiSe}_6$ crystal with Ag1 vacancy is lower in direction parallel to a (see Table 5). The investigated $\text{Ag}_2\text{In}_2\text{GeSe}_6$ crystals with A1 vacancies are favourable for the photovoltaic application and their properties in photoinduced charge recombination are better than it is observed for $\text{Ag}_2\text{In}_2\text{SiSe}_6$ crystal with Ag1 vacancies. The high electrons and holes effective mass calculated theoretically is in agreement to the results obtained experimentally for similar chalcogenide systems⁵⁰⁻⁵².

Conclusions

Following the performed DFT band structure calculations of the $\text{Ag}_2\text{In}_2\text{SiSe}_6$ and $\text{Ag}_2\text{In}_2\text{GeSe}_6$ crystals a principal role of the intrinsic defects in the formation of the optical states localized intra the forbidden energy gap was established. It was found that for both $\text{Ag}_2\text{In}_2\text{SiSe}_6$ and $\text{Ag}_2\text{In}_2\text{GeSe}_6$ structures the cationic vacancies creates the additional energy band located in the energy gap region due to the hybridization of the different orbitals and defects existence.

In presented work the Ag1 and Ag2 cationic vacancies in both structures give the additional energy levels above the valence band but the Ag1 vacancy influence is more pronounced. The occurring discrete energy levels introduced by the Ag1 vacancies are situated 0.34 eV and 0.43 eV above the VBM in $\text{Ag}_2\text{In}_2\text{SiSe}_6$ and $\text{Ag}_2\text{In}_2\text{GeSe}_6$ crystals, respectively. The Ag vacancies in studied semiconductors fulfil a role of acceptor impurities, resulting in an energy increase of acceptor level. One may see that the vacancies named Ag1 and Ag2 have the same formation energy for both structures. Additionally the value of this energy is relatively low and the probability of mentioned vacancies formation is high. More important is an establishment of a fact that Ag vacancies create additional UV-VIS absorption peak in the region of energy gap of the perfect crystal. The intensity of mentioned peak is higher for the $\text{Ag}_2\text{In}_2\text{SiSe}_6$ structure with respect to $\text{Ag}_2\text{In}_2\text{GeSe}_6$. It is in agreement with the experimentally obtained data. For the $\text{Ag}_2\text{In}_2\text{SiSe}_6$ structure the small shoulder at the absorption edge band around 1.55 eV is clearly seen. Mentioned peak is not observed for experimentally investigated $\text{Ag}_2\text{In}_2\text{GeSe}_6$ crystal. It is due to the fact that the theoretically investigated structures are plenty of vacancies and their concentration is higher than it is observed in experiment. One may suppose that for higher concentration of Ag1 or Ag2 vacancies in experimentally investigated $\text{Ag}_2\text{In}_2\text{GeSe}_6$ also the additional absorption peak may be observed.

The anion vacancies as point defects drastically modify the energy band structure of investigated crystals but not modified the optical spectra. The calculated DOS and energy band structure for the Se₆ vacancies reached material may give an impression that also the selenium defects will change significantly the optical properties of the investigated crystals. Unfortunately the calculated absorption spectra look similarly to the one obtained for perfect crystal.

Acknowledgements

Calculations have been carried out in Wroclaw Center for Networking and Supercomputing <<http://www.wcss.wroc.pl>> (Grant no. 171). The MATERIALS STUDIO package was used under POLAND COUNTRY-WIDE LICENSE.

Notes and references

^a Institute of Physics, Jan Dlugosz University, Al. Armii Krajowej 13/15, 42-200 Czestochowa, Poland, Fax: 48 3436 65415; Tel: 48 3436 14919; E-mail m.makowska@ajd.czest.pl (corresponding author)

^b Faculty of Electrical Engineering, Czestochowa University of Technology, Al. Armii Krajowej 17, 42-200 Czestochowa, Poland

^c Physical Faculty, Eastern European University, Voli 6, Lutsk, Ukraine

- 1 Y. Zhang, X. Sun, P. Zhang, X. Yuan, F. Huang and W. Zhang, *J. Appl. Phys.*, 2012, **111**, 063709-6.
- 2 D. B. Khadka and J. H. Kim, *CrystEngComm*, 2013, **15**, 10500-10509.
- 3 O. V. Krykhovets, L. V. Sysa, I. D. Olekseyuk and T. Glowiyak, *J. Alloy. Comp.*, 1999, **287**, 181–184.
- 4 I. D. Olekseyuk, V. P. Sachanyuk and O.V. Parasyuk, *J. Alloy. Comp.*, 2006, **414**, 73–77.
- 5 V. P. Sachanyuk, G. P. Gorgut, V. V. Atuchin, I. D. Olekseyuk and O. V. Parasyuk, *J. Alloy. Comp.*, 2008, **452**, 348–358.
- 6 Y.-K. Chen, M.-C. Chen, L.-J. Zhou, L. Chen and L.-M. Wu, *Inorg. Chem.*, 2013, **52**, 8334–8341.
- 7 I. Chung and M. G. Kanatzidis, *Chem. Mater.*, 2014, **26**, 849–869.
- 8 S. Sharda, N. Sharma, P. Sharma and V. Sharma, *J. Electron. Mater.*, 2013, **42**, 3367-3372.
- 9 Z. Chen, E.-T. Kim and A. Madhukar, *Appl. Phys. Lett.*, 2002, **80**, 2770-2772.
- 10 I. V. Kityk, M. Makowska-Janusik, M. D. Fontana, M. Aillerie, F. Abdi, *Cryst. Res. Technol.*, 2001, **36**, 577-588.
- 11 S. A. Fischer, C. M. Isborn and O. V. Prezhdo. *Chem. Sci.*, 2011, **2**, 400-406.
- 12 K.-H. Kim, J.-C. Park, J.-H. Lee, J.-G. Chung, S. Heo and S.-J. Choi, *Jpn. J. Appl. Phys.* 2010, **49**, 101201-101204.
- 13 G. Myronchuk, S. Danylchuk, O. V. Parasyuk, L. V. Piskach and A. O. Fedorchuk, *Cryst. Res. Technol.*, 2013, **48**, 464–475.
- 14 S. Ozaki, K.-I. Muto, H. Nagata and S. Adachi, *J. Appl. Phys.*, 2005, **97**, 043507-7.
- 15 A. F. Kohan, G. Ceder, D. Morgan and C. G. Van de Walle, *Phys. Rev. B.*, 2000, **61**, 15019-15027.
- 16 F. De Angelis and L. Armelao, *Phys.Chem.Chem.Phys.*, 2011, **13**, 467–475.
- 17 Z. Cheng, T. Liu, C. Yang, H. Gan, F. Zhang and J. Chen, *J. Phys. Chem. Solids*, 2012, **73**, 302–307.
- 18 G.-Y. Huang and B. D. Wirth, *Phys. Rev. B*, 2013, **88**, 085203-16.
- 19 T. Oda, Y. Zhang and W. J. Weber, *J. Chem. Phys.*, 2013, **139**, 124707-16.
- 20 Z. Zhang, P. Wu, L. Lu and C. Shu, *J. Alloy. Comp.*, 2008, **449**, 362–365.
- 21 V. E. Alexandrov, E. A. Kotomin, J. Maier and R. A. Evarestov, *Eur. Phys. J. B*, 2009, **72**, 53–57.
- 22 K. J. Michel and V. Ozolins, *J. Phys. Chem. C*, 2011, **115**, 21443–21453.
- 23 Y. Sharma and P. Srivastava, *Comput. Mat. Science*, 20012, **63**, 451-459.
- 24 F. El Haj Hassan, A. Bleybel, A. Hijazi, A. Alaeddine, B. Beydoun and M. Zoeter, *Mater. Lett.*, 2007, **61**, 1178–1182.
- 25 J. Yao, D. M. Wells, G. H. Chan, H.-Y. Zeng, D. E. Ellis, R. P. Van Duyne and J. A. Ibers, *Inorg. Chem.* 2008, **47**, 6873-6879.
- 26 M. Othman; E. Kasap and N. Korozlu, *J. Alloy. Comp.*, 2010, **496**, 226-230.
- 27 M. Hermus and B. P. T. Fokwa, *Eur. J. Inorg. Chem.*, 2012, **30**, 4877-4884.
- 28 M. Aslan, B. G. Yalc and M. Üstündag, *J. Alloy. Comp.*, 2012, **519**, 55-59.
- 29 F. El Haj Hassan, A. V. Postnikov and O. Pagès, *J. Alloy. Comp.*, 2010, **504**, 559–565.
- 30 L.-J. Zhou, L. Chen, J.-Q. Li and L.-M. Wu, *J. Solid State Chem.*, 2012, **195**, 166–171.
- 31 E. Clementi, D. L. Raimondi and W. P. Reinhardt, *J. Chem. Phys.*, 1963, **38**, 2686-
- 32 S. J. Clark, M. D. Segall, C. J. Pickard, P. J. Hasnip, M. J. Probert, K. Refson and M. C. Payne, *Z. Kristallogr.*, 2005, **220**, 567-570.
- 33 B. G. Pfrommer, M. Cote, S. G. Louie and M. L. Cohen, *J. Comput. Phys.*, 1997, **131**, 233-240.
- 34 J. P. Perdew, K. Burke and M. Ernzerhof, *Phys. Rev. Lett.*, 1996, **77**, 3865-3868.
- 35 A. D. Becke, *Phys. Rev. A*, 1988, **38**, 3098-3100.
- 36 C. Lee, W. Yang and R. G. Parr, *Phys. Rev. B*, 1988, **37**, 785-789.
- 37 D. R. Hamann, M. Schluter and C. Chiang, *Phys. Rev. Lett.*, 1979, **43**, 1494-1497.
- 38 S. Johnsen, S. C. Peter, S. L. Nguyen, J.-H. Song, H. Jin, A. J. Freeman and M. G. Kanatzidis, *Chem. Mater.*, 2011, **23**, 4375–4383.
- 39 M. G. Brik, I. V. Kityk, O. V. Parasyuk and G. L. Myronchuk, *J. Phys.: Condens. Matter*, 2013, **25**, 505802.
- 40 J. Tauc, R. Grigorovici, and A. Vancu, *Phys. Status Solidi B*, 1966, **15**, 627–637.
- 41 J. I. Pankove, *Optical Processes in Semiconductors*, Second Edition, Dover Publications, 2010, p. 448.
- 42 B. Tell, J. L. Shay and H. M. Kasper, *J. Appl. Phys.*, 1972, **43**, 2469–2470.
- 43 E. Hauschild and C. Kannewurf, *J. Phys. Chem. Solids*, 1969, **30**, 353-357.
- 44 W. Setyawan and S. Curtarolo, *Comput. Mater. Sci.*, 2010, **49**, 299-312.
- 45 D. E. Aspnes, J. C. Phillips, K. L. Tai and P. M. Bridenbaugh, *Phys. Rev. B*, 1981, **23**, 816–812.
- 46 H. Iikura, T. Tsuneda, T. Yanai and K. Hirao, *J. Chem. Phys.* 2001, **115**, 3540-3544.
- 47 S. Poykko and D. J. Chadi, *Appl. Phys. Lett.*, 2000, **76**, 499-501.

- 48 D. B. Laks, C. G. Van de Walle, G. F. Neumark, and S. T. Pantelides, *Phys. Rev. Lett.*, 1991, **66**, 648-651.
- 49 S. Tongay, J. Suh, C. Ataca, W. Fan, A. Luce, J. S. Kang, J. Liu, C. Ko, R. Raghunathanan, J. Zhou, F. Ogletree, J. Li, J. C. Grossman and J. Wu, *Sci. Rep.*, 2013, **3**, 2657-5.
- 50 S. N. Guin, A. Chatterjee, K. Biswas, *RSC Advances*, 2014, **4**, 11811-11815.
- 51 S. N. Guin, D. S. Negi, R. Datta, K. Biswas, *J. Mater. Chem. A*, 2014, **2**, 4324-4331.
- 52 S. N. Guin, A. Chatterjee, D. S. Negi, R. Datta, K. Biswas, *Energy Environ. Sci.*, 2013, **6**, 2603-2608.